ACS central science

Research Article

http://pubs.acs.org/journal/acscii

Homogenous Electrocatalytic Oxygen Reduction Rates Correlate with Reaction Overpotential in Acidic Organic Solutions

Michael L. Pegis,[†] Bradley A. McKeown,[†] Neeraj Kumar,[‡] Kai Lang,[§,∥] Derek J. Wasylenko,[⊥,#] X. Peter Zhang,[¶] Simone Raugei,[‡] and James M. Mayer*[,†]

[†]Department of Chemistry, Yale University, New Haven, Connecticut 06520, United States
[‡]Pacific Northwest National Laboratory (PNNL), Richland, Washington 99352, United States
[⊥]Department of Chemistry, University of Washington, Seattle, Washington 98195-1700, United States
[§]Department of Chemistry, University of South Florida, Tampa, Florida 33620, United States
[¶]Department of Chemistry, Merkert Chemistry Center, Boston College, Chestnut Hill, Massachusetts 02467, United States

Supporting Information

ABSTRACT: Improved electrocatalysts for the oxygen reduction reaction (ORR) are critical for the advancement of fuel cell technologies. Herein, we report a series of 11 soluble iron porphyrin ORR electrocatalysts that possess turnover frequencies (TOFs) from 3 s^{-1} to an unprecedented value of 2.2 × 10^6 s^{-1}. These TOFs correlate with the ORR overpotential, which can be modulated by changing the $E_{1/2}$ of the catalyst using different ancillary ligands, by changing the solvent and solution acidity, and by changing the catalyst's protonation state. The overpotential is well-defined for these homogeneous electrocatalysts by the $E_{1/2}$ of the catalyst and the proton activity of the solution. This is the first such correlation for homogeneous ORR electrocatalysis, and it demonstrates that the remarkably fast TOFs are a consequence of high overpotential. The correlation with overpotential is surprising since the turnover limiting steps involve oxygen binding and protonation, as opposed to turnover limiting electron transfer commonly found in Tafel analysis of heterogeneous ORR materials. Computational studies show that the free energies for oxygen binding to the catalyst and for protonation of the superoxide complex are in general linearly related to the catalyst $E_{1/2}$, and that this is the origin of the overpotential correlations. This analysis thus provides detailed understanding of the ORR barriers. The best catalysts involve partial decoupling of the influence of the second coordination sphere from the properties of the metal center, which is suggested as new molecular design strategy to avoid the limitations of the traditional scaling relationships for these catalysts.

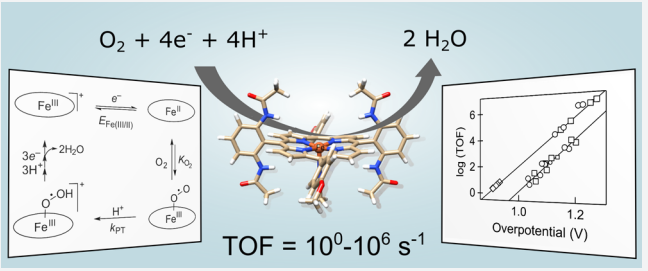

INTRODUCTION

Fuel cells offer clean and effective electrical power generation from chemical fuels for stationary, portable, and transport applications.[1] Widespread implementation of fuel cell technologies has been limited in large part by the inefficient oxygen reduction reaction (ORR) at the cathode, and by the typical requirement for large amounts of expensive platinum.[2,3] This motivates research in heterogeneous and homogeneous catalysts, from new platinum alloy nanocrystals supported on electrodes[4] to novel earth-abundant carbonaceous materials[5] to unique molecular structures and hybrid combinations.[6,7] Homogeneous electrocatalysts have yet to match heterogeneous materials in turnover frequencies (TOFs) per active site at modest overpotentials, but they permit facile development of important structure/activity and driving force/activation barrier relationships. Such atomic-level understanding is key to building better ORR electrocatalysts.

Iron and cobalt complexes with N_4-macrocyclic ligands have been extensively studied as ORR catalysts[8,9] and are models for promising but complex solid Fe/N/C ORR electrodes.[10] Molecular ORR electrocatalysts are typically only soluble in organic solvents such as *N*,*N*′-dimethylformamide (DMF) or acetonitrile (ACN), making it difficult to directly compare and understand the effects of different design features. In addition, the standard potentials for O_2/H_2O in nonaqueous solvents were unknown until recently.[11,12] Therefore, previous studies have predominantly done aqueous measurements of molecular ORR electrocatalysts adsorbed on electrodes, often in complex pastes. In these situations, differing local environments complicate understanding,[13] with some elegant exceptions.[7,14]

Described here are studies on a series of 11 iron porphyrin ORR electrocatalysts ([Fe^{III}(por)]OTf with OTf = trifluoromethanesulfonate, Figure 1A). Catalysts **1** and **8**−**11** were designed with pendant functionalities to serve as potential "proton relays", with the aim of facilitating H^+ delivery to the iron active site. This has been shown to be an effective strategy for other homogeneous electrocatalysts for H^+ and CO_2

Received: September 1, 2016
Published: October 28, 2016

DOI: 10.1021/acscentsci.6b00261
ACS Cent. Sci. 2016, 2, 850−856

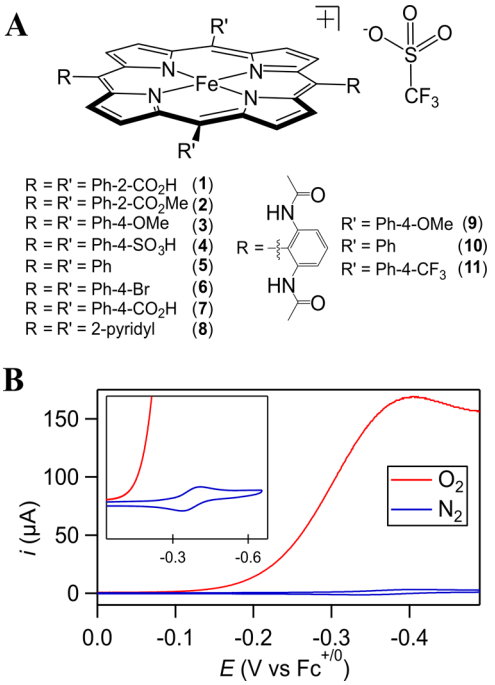

Figure 1. (A) Iron(III) 5,10,15,20-tetraarylporphyrin electrocatalysts **1**–**11**. (B) CV of **1** in ACN under 1 atm of N_2 (blue) or O_2 (red), 20 mM [DMF-H]OTf, 100 mV/s scan rate; the inset shows the electrocatalytic onset (foot-of-the-wave) region.

reduction.[15,16] The catalysts were electrochemically evaluated for homogeneous ORR in organic solvents, with varying amounts of acid. Analysis of the ORR turnover frequencies shows strong correlations with the recently available standard potentials[11,12] under the differing conditions. This is the first such analysis for molecular ORR catalysts. The presence of the correlations is remarkable because the turnover limiting steps for these catalysts do not involve electron transfer from the electrode. Computational analysis of a subset of the catalysts shows that the correlation with overpotentials results from linear free energy relationships connecting the catalyst $E_{1/2}$ with its O_2 binding free energy and the proton affinity of the resulting superoxide complex, providing atomic-level understanding of this series of electrocatalysts.

RESULTS

The electrochemistry of complexes **1**–**11** has been examined in DMF or ACN, with excess [DMF-H]OTf as the acid. Most catalysts could only be evaluated in one of these solvents, due to limited solubility. Cyclic voltammograms (CVs) of the complexes all showed a reversible $Fe^{III/II}$ redox couple in the absence of O_2. Changing the substituents on the porphyrin scaffold allowed tuning of the $Fe^{III/II}$ reduction that initiates electrocatalysis ($E_{Fe(III/II)}$) over a significant range in ACN (~100 mV) and DMF (~270 mV). In the presence of excess acid and 1 atm of O_2, CVs of **1**–**11** showed a substantial increase in current, indicative of ORR electrocatalysis (Figure 1B).

Turnover frequencies (TOFs, s^{-1}) were quantified electrochemically using foot-of-the-wave analysis (FOWA; see Supporting Information). This TOF is defined by the rate law $-d[O_2]/dt = TOF[Fe^{II}]$, as is common;[16,17] it corresponds to the more electrochemically precise TOF_{max} recently introduced by Savéant et al.[18,19] FOWA enables determination

Table 1. Catalyst Reduction Potentials (vs Ferrocene/Ferrocenium, $Fc^{+/0}$), ORR Overpotentials (See Text), and TOF from FOWA[a]

catalyst	$E_{Fe(III/II)}$ (V)	$\eta_{Fe/ORR}$ (V)	TOF (s^{-1})
1^{ACN}	−0.375	1.21	2.2×10^6
2^{ACN}	−0.390	1.24	2.2×10^6
9^{ACN}	−0.326	1.15	6.5×10^4
10^{ACN}	−0.296	1.13	2.2×10^4
11^{ACN}	−0.280	1.11	2.2×10^2
1^{DMF}	−0.630	1.18	2.0×10^3
2^{DMF}	−0.611	1.16	2.5×10^3
3^{DMF}	−0.547	1.10	1.6×10^2
4^{DMF}	−0.536	1.09	1.8×10^2
5^{DMF}	−0.530	1.08	2.7×10^1
6^{DMF}	−0.491	1.04	5.0×10^0
7^{DMF}	−0.486	1.04	1.5×10^1
8^{DMF}	−0.362	0.91	3.0×10^0

[a]In ACN (superscript "ACN") or DMF (superscript "DMF"), 0.1 M $[Bu_4N]PF_6$, 1 atm of O_2, 20 mM [DMF-H]OTf, 100 mV/s scan rate. Experimental uncertainties are ±5 mV for $E_{Fe(III/II)}$, ±20 mV for overpotentials, and ±15% for TOFs.

of TOFs for soluble electrocatalysts despite limitations such as substrate consumption and catalyst decomposition.[18] The TOFs in the presence of 1 atm of O_2 and 20 mM [DMF-H]OTf are given in Table 1. The TOFs in general increase linearly with increasing partial pressures of O_2 and [DMF-H]OTf (Figures S1 and S20–S32). The TOF values reported in Table 1 are in regions where the TOF scales linearly with the [DMF-H^+], however some catalysts become independent of the acid strength at higher concentrations (see below). In general, the TOF (or TOF_{max}[18,19]) values are well-defined properties of the molecular catalysts. For the catalysts studied here, the rate of O_2 consumption near the electrode surface (and thus current, Figure 1B) reaches a plateau when $E < E_{1/2}$, representing the maximum chemical rate under conditions where electron transfer from the electrode to the soluble catalyst is rapid and complete.[18] This is in contrast to heterogeneous electrocatalysts where the current typically continues to increase exponentially with the applied potential. The effective overpotential for different molecular electrocatalysts can then be defined by the potential of the catalysis-initiating redox couple (in this case the $E_{1/2}$ of $Fe^{III/II}$, $E_{Fe(III/II)}$) and the ORR equilibrium potential under the relevant catalytic conditions (O_2 pressure, proton and water activity).[12]

Catalyst selectivity was investigated by electrochemical detection of hydrogen peroxide using rotating ring disk voltammetry (RRDV, see Supporting Information for details). Under identical conditions, **1**–**11** produced minor amounts of hydrogen peroxide (<15% H_2O_2). The % H_2O_2 converts to an average number of electrons transferred per catalytic turnover ($n_{cat} > 3.83$), which has been included in the TOF calculations. Thus, these catalysts are quite selective for the direct reduction of O_2 to H_2O, as has been previously reported for iron porphyrin complexes under similar conditions.[20,21]

The 2-carboxyphenyl catalyst (**1**) and its methyl ester (**2**) are both remarkably fast catalysts in ACN solution, with TOFs of 2.2×10^6 s^{-1} for both systems under our standard conditions (Table 1). Contributions from adsorbed or heterogenized catalysis on the electrode surface were found to be negligible through use of a rinse test (Figure S18). The catalytic rate of O_2 reduction by **1** was also examined by a nonelectrochemical

DOI: 10.1021/acscentsci.6b00261
ACS Cent. Sci. 2016, 2, 850–856

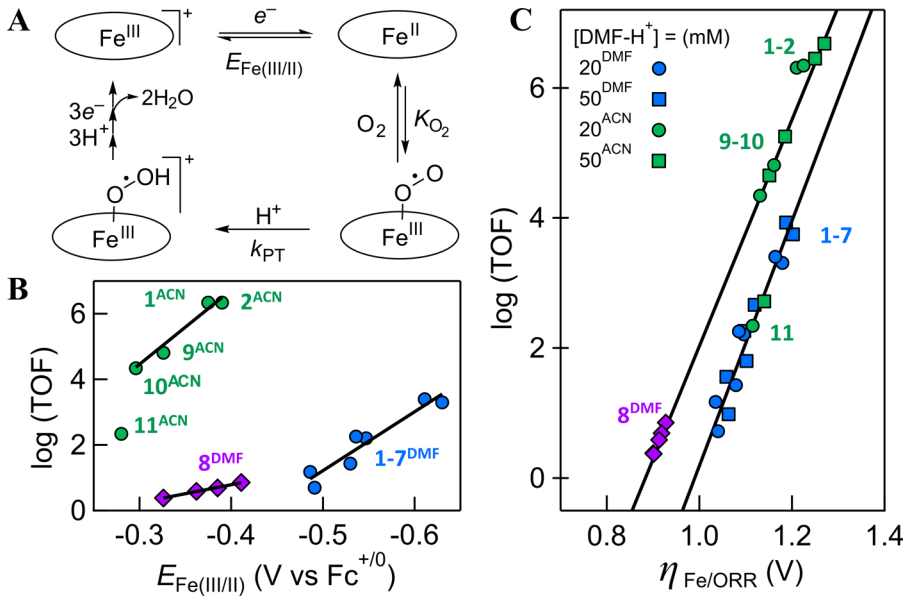

Figure 2. (A) Proposed initial steps in the ORR catalyzed by **1**−**11** (oval = porphyrin). (B) log(TOF) as a function of $E_{Fe(III/II)}$ with 20 mM [DMF-H]OTf, 1 atm of O_2. The four purple points for $\mathbf{8}^{DMF}$ correspond to (from left to right) 50, 20, 10, and 5 mM [DMF-H$^+$]OTf. (C) log(TOF) as a function of the catalyst-specific overpotential $\eta_{Fe/ORR}$ (defined at catalyst $E_{1/2}$, see text). The solvent and acid concentrations are indicated by the color and shape of the points, as indicated in the legend. Groups of points are labeled by the catalyst numbers in that group. $\mathbf{8}^{DMF}$ is represented in purple, and the conditions are identical to those specified in panel B.

stopped-flow kinetics study (see Supporting Information). Following our earlier methodology,[22] an ACN solution of 3 μM **1**, 8 mM Cp^*_2Fe (Cp^* = pentamethylcyclopentyldienyl), and 2.2 mM [DMF-H]OTf/2.2 mM DMF was mixed with an air-saturated O_2 solution. The appearance of $[Cp^*_2Fe]^+$ was complete within 200 ms (Figure S46). Converting the derived third order rate constant to a TOF under the electrochemical conditions gives TOF = 1.1 × 10^6 s^{-1}. Thus, spectrochemical kinetic measurements are consistent with the electrochemical results and provide confirmation of the remarkably high catalytic activities observed.

The TOFs for **1** and **2** in ACN are, to our knowledge, the fastest TOFs ever reported for homogeneous ORR electrocatalysts. Furthermore, the TOFs for **1** and **9** increase linearly with [DMF-H]$^+$ until saturation kinetics are observed at higher acid concentrations and the TOFs become independent of [DMF-H]$^+$. The maximum TOFs are 3 × 10^6 s^{-1} and 2.5 × 10^5 s^{-1} for **1** and **9**, respectively. Based on the catalytic mechanism in Figure 2A,[22] when the rate becomes independent of acid concentration, the TOF is limited by O_2 binding (see Supporting Information, page 5). Using TOF = $k_{O2}[O_2]$ and $[O_2]$ = 8 mM in ACN under 1 atm of O_2, the saturation TOFs correspond to second order rate constants for O_2 binding, k_{O2} = 4 × 10^8 M^{-1} s^{-1} (**1**) and 3 × 10^7 M^{-1} s^{-1} (**9**). These are in the range of typical k_{O2} for ferrous porphyrins.[8] Thus, these catalysts approach the fastest possible rate, being only ~10^2 below the rate constant for diffusive encounter of O_2 and the catalyst.[23]

The 2-pyridyl substituted complex **8**, unique among the catalysts in the series, displays an *inverse* dependence on the concentration of acid. Increasing the concentration of [DMF-H]OTf causes the TOF for **8** to decrease, and also shifts the $E_{Fe(III/II)}$ to more positive values. This is likely a consequence of increased protonation of the 2-pyridyl substituents upon addition of [DMF-H]OTf. Indeed, under 1 atm of N_2 the $E_{Fe(III/II)}$ for **8** shifts in a Nernstian fashion (90 mV/decade in [DMF-H$^+$], Figure S19) implying that, upon reduction, the average protonation state of **8** increases by one and a half, though detailed characterization of the equilibrium mixture of proteomers and rotamers in solution has not been achieved. Qualitatively, increasing the average protonation state of the catalyst results in less active forms and decreases the TOF.

Initial understanding of the TOFs for the various iron catalysts came from plotting log(TOF) versus $E_{Fe(III/II)}$, which revealed linear free energy relationships (LFERs) within each solvent system (Figure 2B). The LFERs fit very well for each unique system analyzed (R^2 > 0.98, $\mathbf{8}^{DMF}$ excluded due to its unusual acid dependence and $\mathbf{11}^{ACN}$ excluded for reasons described below). The ORR TOFs are larger for catalysts with more negative $E_{Fe(III/II)}$. When the catalyst $E_{Fe(III/II)}$ is more negative, its reduced form is more electron rich (and the TOF reports on the rate under conditions when the catalyst is fully reduced, see above). The log(TOF)/$E_{Fe(III/II)}$ correlation is limited, however, because it focuses only on the electrochemical potential while the ORR is an electron/*proton* process. Thus, this LFER does not account for the differences in proton activity (such as in the case of **8**, where each data point represents the same initial catalyst with varying amounts of [DMF-H$^+$]. In addition, electrochemical potentials are not easily compared between solvents.

It is more appropriate to correlate TOF with the overall driving force of the catalytic reaction. For each of the reaction conditions used here, there is a characteristic equilibrium potential for O_2 reduction ($E_{O2/H2O}$), depending on the solvent, proton activity, etc.[11] Similarly, each of the molecular catalysts has a characteristic redox potential under these conditions ($E_{Fe(III/II)}$), which we approximate as the measured $E_{1/2}$ of the catalyst (see Supporting Information, page 5). We therefore define a characteristic overpotential under these conditions, $\eta_{Fe/ORR} = E_{O2/H2O} - E_{Fe(III/II)}$. This $\eta_{Fe/ORR}$ is the characteristic value within the general definition of overpotential as the difference between $E_{O2/H2O}$ and the applied potential E. We

DOI: 10.1021/acscentsci.6b00261
ACS Cent. Sci. 2016, 2, 850−856

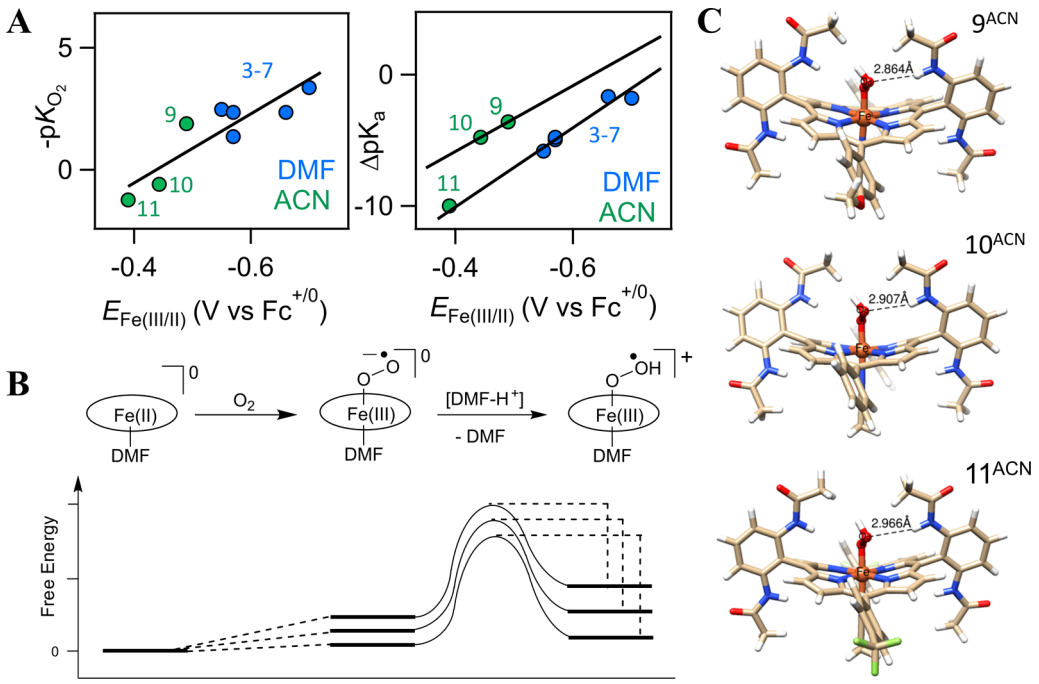

Figure 3. (A) Computed correlations between O_2 binding (pK_{O2}, left) and $pK_a[Fe^{III}(por)(O_2^{\bullet}H)]^+ - pK_a[DMF\text{-}H]^+$ (right) vs $E_{Fe(III/II)}$. (B) Reaction coordinate qualitatively depicting the barrier height change as a function of driving force for proton transfer. (C) Optimized structures of $[Fe^{III}(por)(O_2^{\bullet}H)]^+$ for **9**–**11**^{ACN}, depicting the changes in NH···O hydrogen bond length.

emphasize that $\eta_{Fe/ORR}$ is a well-defined single value for a molecular electrocatalyst, because the current density (and thus reaction rate) are constant at overpotentials beyond $E_{Fe(III/II)}$.[24] This contrasts with the situation for heterogeneous electrocatalysts, where the current density increases exponentially with η.

Correlating log(TOF) with $\eta_{Fe/ORR}$ for the 11 catalysts analyzed in different conditions shows that all of the results fall on two parallel lines (Figure 2C). The simple relationship between TOF and $\eta_{Fe/ORR}$ has been independently observed in three different ways: (i) changing the catalyst, which changes $E_{Fe(III/II)}$; (ii) changing the solvent, which alters $E_{O2/H2O}$; and (iii) changing the $[DMF\text{-}H]^+$, which shifts $E_{O2/H2O}$ in a Nernstian fashion. Catalyst **8** is unique since both i and iii occur upon changing the $[DMF\text{-}H]^+$. Considering both changes for **8** in Figure 2C places all of its values on a LFER of similar slope to catalysts **1**–**7** in DMF. This analysis allows, for the first time, the direct comparison of homogeneous ORR electrocatalysts in different solvents and with different acid concentrations. Thus, catalysts **1**, **2**, **9**, and **10** in ACN and **8** in DMF are clearly better catalysts than the other, because they lie on a line that is above and to the left. At a given $\eta_{Fe/ORR}$, the catalyst systems on the left line have higher TOFs, or stated another way, these catalysts require a lower $\eta_{Fe/ORR}$ to reach the same TOF.

Dissecting the TOF/$\eta_{Fe/ORR}$ correlations provides additional understanding. The log(TOF) vs $\eta_{Fe/ORR}$ lines in Figure 2C have inverse slopes of 57 and 54 mV per decade in TOF for the left and right correlations, respectively. This is (by coincidence we believe) remarkably close to the Nernstian slope of 59 mV per decade in concentration. We emphasize that this plot is distinct from the traditional Tafel plot analysis of a *single* electrocatalyst at different applied potentials (molecular or heterogeneous). Figure 2C relates the properties of *different* catalysts under *different* conditions. Fundamentally, these correlations show how the barrier height of turnover limiting step(s) changes as a function of overall driving force, varied via $E_{O2/H2O}$, $E_{Fe(III/II)}$, or both for **8**.

The presence of these correlations is remarkable. For these catalysts, the measured TOF is limited by the O_2 binding equilibrium and the rate of protonation of the superoxide intermediate, as shown in the mechanism in Figure 2A. The TOFs are not determined by any electrochemical step. The correlations indicate that electronic modifications of the catalysts linearly tune the free energies of the relevant intermediates and reaction steps of the catalytic cycle.

This tuning is revealed by density functional theory (DFT) calculations of the reduction potentials $E_{Fe(III/II)}$, O_2 binding equilibrium constants pK_{O2}, and the pK_as of the protonated superoxide intermediate ($[Fe^{III}(por)(O_2^{\bullet}H)]^+$). All of the catalysts were calculated except for **1**, **2**, and **8**, for which many rotamers exist in solution. The pK_a of the protonated superoxide intermediate ($[Fe^{III}(por)(O_2^{\bullet}H)]^+$) is directly related to the free energy of protonation of the superoxide, the rate-determining step. The calculations show clear correlations among the computed catalyst $E_{Fe(III/II)}$, the pK_{O2}s, and the pK_as (Figure 3). Electron donating substituents that shift $E_{Fe(III/II)}$ to more negative values increase the O_2 affinity and the superoxide basicity, increasing the TOF. Quantitatively, using simple transition state theory and Bell–Polanyi–Evans (BPE) arguments, it is possible to show that $\log(TOF) = -pK_{O2} + \alpha \cdot pK_a + C$. Taking $\alpha = 1/2$ (see Supporting Information), the computations predict a LFER of 43 mV/decade in TOF, in good agreement with the experimental value.[25] For $\alpha = 0.23$, computations and experiments match exactly.

The correlations and calculated energetics of elementary steps demonstrate that installing pendant protic or hydrogen bond donor/acceptor functionalities in the second coordination sphere (i.e., **1**, **8**–**11**) in most cases has a negligible effect on the TOFs for the ORR. The 2-carboxylic acid catalyst **1**^{DMF} has

DOI: 10.1021/acscentsci.6b00261
ACS Cent. Sci. 2016, 2, 850–856

a higher TOF than the isomeric 4-carboxylic acid isomer 7^{DMF} (2040 s^{-1} vs 15 s^{-1} in DMF) simply because **1** has the more negative reduction potential. Catalyst **1** and its methyl ester **2** have $E_{Fe(III/II)}$ values within 19 mV and very close TOFs (within 20%), in both ACN and DMF, even though only **1** would appear to have proton relays. The presence of potential proton relays does not displace the pK_{O2} and the pK_a of the catalyst from the correlation lines. This conclusion contrasts with the great value of such "proton relays" in electrocatalysts for H^+ and CO_2 reduction[15,16] and shows that the observation of improved rates for catalysts containing potential relays does not demonstrate a relay effect.

The lack of a "relay effect" arises from a thermodynamic mismatch; the pendant proton donors (PyH^+, $PhCO_2H$) are not strong enough to protonate $[Fe^{III}(por)(O_2^{\bullet})]$. Using extrapolated values from Figure 3A for $\mathbf{1}^{DMF}$ and $\mathbf{1}^{ACN}$, this mismatch may be >12 pK_a units. The proton must be delivered from the much stronger $[DMF\text{-}H]^+$ acid in solution, which is the proton source in both DMF and ACN solvents. While there is no definitive evidence for intramolecular proton transfer in these systems, the second coordination sphere may play a noninnocent role in defining the TOF/η correlations. Such is the case for catalysts **9**−**11**. Despite all having identical ortho-amide NH groups[26] that are highly pK_a-*mismatched* with the external acid, catalysts **9** and **10** fall upon a more efficient TOF/η correlation than **11**, discussed below.

Figure 2C shows two LFER lines of nearly identical slope for this set of catalysts and conditions. The lower η line (to the left) primarily has the systems in ACN, suggesting that this is the better solvent for ORR in general, but $\mathbf{8}^{DMF}$ falls on that line and $\mathbf{11}^{ACN}$ falls on the higher η line with most of the systems in DMF. As emphasized above, the TOFs are limited by O_2 binding and the subsequent superoxide ligand protonation. Computationally, there is a single correlation between pK_{O2} and $E_{Fe(III/II)}$ that includes all of the catalysts in both solvents (slope ∼100 mV/unit pK_{O2}, Figure 3A, left). Therefore, this is not the origin of the better catalysis by **9** and **10**. Their advantage originates solely from their better proton transfer thermodynamics, as their protonated superoxide complexes have higher pK_a values than would be expected from their $E_{Fe(III/II)}$ (Figure 3A, right). Indeed, **9** and **10** have the most favorable $\Delta G°$ for proton transfer (−3.5 and −1.8 kcal/mol, respectively) of all catalysts analyzed. They are easier to protonate and have higher TOFs. We suspect that similar issues explain why **1**, **2**, and **8** fall on the better correlation line, but their complicated mixture of rotamers precluded computational analysis, as noted above. The related CF_3-substituted amide catalyst **11** does not have this elevated pK_a and does not have the elevated TOF (it falls on the LFER line to the right).

To further understand the origin of the distinct p*K*a values for the amide catalysts **9**−**11**, we compared the optimized structures of the relevant intermediates. There is a hydrogen bond from the amide NH groups in the second coordination sphere to the distal O (O_d) of the O_2-derived ligand (Figure 3C). In principle, the hydrogen bonds should be strongest—greatest stabilization by the second coordination sphere—for the more electron rich intermediates. Indeed, for the protonated superoxide complexes $[Fe^{III}(por)(O_2^{\bullet}H)]^+$, the calculations show that the intermediate from **9** has the shortest NH−O distance, nearly 0.1 Å shorter than that in **11**: d(NH−O_d) = 2.864 Å, 2.907 Å, and 2.966 Å for **9**−**11**, respectively. However, the trend is the opposite when comparing the NH−O distances of the $[Fe^{III}(por)(O_2^{\bullet})]$ intermediates, where the NH−O_d distances are 2.379 Å, 2.361 Å, and 2.296 Å for **9**−**11**, respectively (see Figure S72). Therefore, proton transfer to form $[Fe^{III}(por)(O_2H^{\bullet})]^+$ requires the largest changes in the NH−O distance for **11** (0.670 Å) when compared to **10** and **9** (0.546 and 0.485 Å). Given that the majority of the other bond lengths and angles are quite similar for **9**−**11**, the NH−O hydrogen bond seems to play an important role in modulating the $E_{1/2}$ to pK_a (and thus TOF) relations. The stronger H-bonding interaction for the protonated superoxide complexes **9** and **10** allow for a more exoergic proton transfer, resulting in TOFs roughly 2 orders of magnitude larger than **11** under identical conditions (after correcting for the difference in overpotentials). This H-bonding effect of the "relay" was unexpected since the proton is delivered from the exogenous donor, [DMF-H^+]. Differences in proton transfer energetics may also be the reason for **1** and **2** behaving so much better in ACN than DMF, and also for **8** compared to **1**−**7**. Understanding the better catalysis by these complexes is challenging because of the presence of multiple conformations and/or protonation states. The selective stabilization of one intermediate over another for **9** and **10** is an effect of the second coordination sphere groups, due to hydrogen bonding rather than proton delivery. The occurrence of this effect for complexes **9** and **10** but not for **11** shows the subtle interplay of factors contributing to such second coordination sphere effects.

The combined experimental and theoretical studies reported herein provide a detailed look at the factors that underlie molecular ORR electrocatalysis. Changing substituents on the aryl rings of these metalloporphyrin catalysts changes their $E_{Fe(III/II)}$, and all of the key parameters change in parallel for most of the catalysts. This approach of finding linear free energy relationships is the same principle that has become a primary way to analyze sets of heterogeneous catalysts, including electrocatalysts.[27] The widely used "volcano plots" and "scaling relationships" correlate catalyst activity with a single descriptor such as a surface−substrate binding energy or the d-band center, and the relationships hold when the free energies of the different catalytic steps scale linearly with the descriptor. A recent computational study of iron porphyrin ORR catalysts showed the presence of scaling relations for the binding of OH, O, and OOH, but did not consider separate electron or proton transfer steps.[28] The combined experimental and computational study reported here provides a more detailed analysis and shows one way to overcome the scaling relationships. Further studies are in progress to design improved catalysts by further decoupling the properties of the second coordination sphere from those of the first. This is a new design principle for catalysis of multielectron/multiproton reactions.

The results and analysis developed here allow, for the first time, comparisons of molecular O_2 reduction electrocatalysts under diverse conditions. The correlations observed in this study show that the ORR activities for catalysts **1**−**11** correlate with the well-defined overpotentials (η) for these molecular catalysts under a range of conditions, on two parallel linear free energy relationships. The correlations hold for a variety of electrocatalysts and media across 6 orders of magnitude in TOF, and show that the extraordinarily high TOFs for **1** and **2**, close to the diffusion limit for the $4e^-/4H^+$ ORR reaction, are mostly due to their high η. These correlations are shown computationally to stem from the chemical steps of O_2 binding and proton transfer. The origin of the improved behavior of some of the electrocatalysts is shown to derive from deviations

DOI: 10.1021/acscentsci.6b00261
ACS Cent. Sci. 2016, 2, 850−856

in the correlation of catalyst properties ($E°$, K_{O2}) with the basicity of the superoxide intermediate (pK_a[Fe(por)-$(O_2^{\bullet}H)^+$]). This concept of decoupling the thermochemical properties of the first and second coordination spheres is a new approach to catalyst design.

■ ASSOCIATED CONTENT

Supporting Information

The Supporting Information is available free of charge on the ACS Publications website at DOI: 10.1021/acscentsci.6b00261.

Synthesis procedures, characterization, and calculations (PDF)

■ AUTHOR INFORMATION

Corresponding Author

*E-mail: james.mayer@yale.edu.

Present Addresses

[‖]K.L.: Department of Chemistry, Merkert Chemistry Center, Boston College, Chestnut Hill, MA 02467

[#]D.J.W.: NOVA Chemicals Corp., Calgary, AB T1Y 6G7, Canada.

Notes

The authors declare no competing financial interest.

■ ACKNOWLEDGMENTS

This research was supported as part of the Center for Molecular Electrocatalysis, an Energy Frontier Research Center funded by the U.S. Department of Energy (DOE), Office of Science, Office of Basic Energy Sciences. The National Science Foundation (CHE-1624216) funded synthesis of porphyrin ligands for **9**−**11**. Computational resources were provided by the National Energy Research Computing Center (NERSC) at the Lawrence Berkeley National Laboratory and W. R. Wiley Environmental Molecular Sciences Laboratory (EMSL), a national scientific user facility sponsored by the Department of Energy's Office of Biological and Environmental Research located at Pacific Northwest National Laboratory.

■ REFERENCES

(1) Winter, M.; Brodd, R. J. What Are Batteries, Fuel Cells, and Supercapacitors? *Chem. Rev.* **2004**, *104*, 4245−4269.

(2) Wang, S.; Zhang, L.; Xia, Z.; Roy, A.; Chang, D. W.; Baek, J. B.; Dai, L. BCN Graphene as Efficient Metal-Free Electrocatalyst for the Oxygen Reduction Reaction. *Angew. Chem., Int. Ed.* **2012**, *51*, 4209−4212.

(3) Gasteiger, H. A.; Kocha, S. S.; Sompalli, B.; Wagner, F. T. Activity Benchmarks and Requirements for Pt, Pt-Alloy, and Non-Pt Oxygen Reduction Catalysts for PEMFCs. *Appl. Catal., B* **2005**, *56*, 9−35.

(4) Wu, J.; Yang, H. Platinum-Based Oxygen Reduction Electrocatalysts. *Acc. Chem. Res.* **2013**, *46*, 1848−1857.

(5) Dai, L.; Xue, Y.; Qu, L.; Choi, H.-J.; Baek, J.-B. Metal-Free Catalysts for Oxygen Reduction Reaction. *Chem. Rev.* **2015**, *115*, 4823−4892.

(6) McGuire, R., Jr.; Dogutan, D. K.; Teets, T. S.; Suntivich, J.; Shao-Horn, Y.; Nocera, D. G. Oxygen Reduction Reactivity of Cobalt(II) Hangman Porphyrins. *Chem. Sci.* **2010**, *1*, 411−414.

(7) Barile, C. J.; Tse, E. C. M.; Li, Y.; Sobyra, T. B.; Zimmerman, S. C.; Hosseini, A.; Gewirth, A. A. Proton Switch for Modulating Oxygen Reduction by a Copper Electrocatalyst Embedded in a Hybrid Bilayer Membrane. *Nat. Mater.* **2014**, *13*, 619−623.

(8) Jones, R. D.; Summerville, D. A.; Basolo, F. Synthetic Oxygen Carriers Related to Biological Systems. *Chem. Rev.* **1979**, *79*, 139−179.

(9) Collman, J. P.; Boulatov, R.; Sunderland, C. J.; Fu, L. Functional Analogues of Cytochrome c Oxidase, Myoglobin, and Hemoglobin. *Chem. Rev.* **2004**, *104*, 561−588.

(10) Lefèvre, M.; Proietti, E.; Jaouen, F.; Dodelet, J.-P. Iron-Based Catalysts with Improved Oxygen Reduction Activity in Polymer Electrolyte Fuel Cells. *Science* **2009**, *324*, 71−74.

(11) Pegis, M. L.; Roberts, J. A. S.; Wasylenko, D. J.; Mader, E. A.; Appel, A. M.; Mayer, J. M. Standard Reduction Potentials for Oxygen and Carbon Dioxide Couples in Acetonitrile and *N*,*N*-Dimethylformamide. *Inorg. Chem.* **2015**, *54*, 11883−11888.

(12) Passard, G.; Ullman, A. M.; Brodsky, C. N.; Nocera, D. G. Oxygen Reduction Catalysis at a Dicobalt Center: The Relationship of Faradaic Efficiency to Overpotential. *J. Am. Chem. Soc.* **2016**, *138*, 2925−2928.

(13) Rigsby, M. L.; Wasylenko, D. J.; Pegis, M. L.; Mayer, J. M. Medium Effects Are as Important as Catalyst Design for Selectivity in Electrocatalytic Oxygen Reduction by Iron-Porphyrin Complexes. *J. Am. Chem. Soc.* **2015**, *137*, 4296−4299.

(14) Collman, J. P.; Devaraj, N. K.; Decréau, R. A.; Yang, Y.; Yan, Y.-L.; Ebina, W.; Eberspacher, T. A.; Chidsey, C. E. D. A Cytochrome *c* Oxidase Model Catalyzes Oxygen to Water Reduction under Rate-Limiting Electron Flux. *Science* **2007**, *315*, 1565−1568.

(15) Costentin, C.; Drouet, S.; Robert, M.; Savéant, J.-M. A Local Proton Source Enhances CO_2 Electroreduction to CO by a Molecular Fe Catalyst. *Science* **2012**, *338*, 90−94.

(16) Helm, M. L.; Stewart, M. P.; Bullock, R. M.; DuBois, M. R.; DuBois, D. L. A Synthetic Nickel Electrocatalyst with a Turnover Frequency above 100,000 s^{-1} for H_2 Production. *Science* **2011**, *333*, 863−866.

(17) Appel, A. M.; Helm, M. L. Determining the Overpotential for a Molecular Electrocatalyst. *ACS Catal.* **2014**, *4*, 630−633.

(18) Costentin, C.; Drouet, S.; Robert, M.; Savéant, J.-M. Turnover Numbers, Turnover Frequencies, and Overpotential in Molecular Catalysis of Electrochemical Reactions. Cyclic Voltammetry and Preparative-Scale Electrolysis. *J. Am. Chem. Soc.* **2012**, *134*, 11235−11242.

(19) Artero, V.; Saveant, J.-M. Toward the Rational Benchmarking of Homogeneous H_2-Evolving Catalysts. *Energy Environ. Sci.* **2014**, *7*, 3808−3814.

(20) Shigehara, K.; Anson, F. C. Electrocatalytlc Actlvlty of Three Iron Porphyrins in the Reductions of Dioxygen and Hydrogen Peroxide at Graphite Electrodes. *J. Phys. Chem.* **1982**, *86* (14), 2776−2783.

(21) Carver, C. T.; Matson, B. D.; Mayer, J. M. Electrocatalytic Oxygen Reduction by Iron Tetra-Arylporphyrins Bearing Pendant Proton Relays. *J. Am. Chem. Soc.* **2012**, *134*, 5444−5447.

(22) Wasylenko, D. J.; Rodriguez, C.; Pegis, M. L.; Mayer, J. M. Direct Comparison of Electrochemical and Spectrochemical Kinetics for Catalytic Oxygen Reduction. *J. Am. Chem. Soc.* **2014**, *136*, 12544−12547.

(23) Andrieux, C. P.; Blocman, C.; Dumas-Bouchiat, J. M.; M'Halla, F.; Saveant, J. M. Determination of the Lifetimes of Unstable Ion Radicals by Homogeneous Redox Catalysis of Electrochemical Reactions. Application to the Reduction of Aromatic Halides. *J. Am. Chem. Soc.* **1980**, *102*, 3806−3813.

(24) Molecular Tafel plot analysis considers the TOF to be defined per *total* catalyst confined in the reaction diffusion layer, leading to a Nernstian relationship between TOF and overpotential (see refs 17 and 19). This analysis is useful for comparing molecular TOFs to heterogeneous catalysts, where the relationship between active and inactive catalytic forms is often unquantifiable.

(25) The proton transfer coefficient (α) was experimentally measured as 0.3, resulting in excellent agreement between experiment (54 and 57 mV/dec) and theory (50 mV/dec) and is the subject of future publication.

(26) Chen, Y.; Fields, K. B.; Zhang, X. P. Bromoporphyrins as Versatile Synthons for Modular Construction of Chiral Porphyrins: Cobalt-Catalyzed Highly Enantioselective and Diastereoselective Cyclopropanation. *J. Am. Chem. Soc.* **2004**, *126*, 14718−14719.

DOI: 10.1021/acscentsci.6b00261
ACS Cent. Sci. 2016, 2, 850−856

(27) Medford, A. J.; Vojvodic, A.; Hummelshøj, J. S.; Voss, J.; Abild-Pedersen, F.; Studt, F.; Bligaard, T.; Nilsson, A.; Nørskov, J. K. From the Sabatier Principle to a Predictive Theory of Transition-Metal Heterogeneous Catalysis. *J. Catal.* **2015**, *328*, 36−42.
(28) Baran, J. D.; Grönbeck, H.; Hellman, A. Analysis of Porphyrines as Catalysts for Electrochemical Reduction of O_2 and Oxidation of H_2O. *J. Am. Chem. Soc.* **2014**, *136*, 1320−1326.

DOI: 10.1021/acscentsci.6b00261
ACS Cent. Sci. 2016, 2, 850−856